ChemComm

COMMUNICATION

View Article Online
View Journal | View Issue

Cite this: *Chem. Commun.*, 2015, **51**, 17728

Received 3rd August 2015,
Accepted 15th October 2015

DOI: 10.1039/c5cc06480e

www.rsc.org/chemcomm

Nanogold supported on manganese oxide doped alumina microspheres as a highly active and selective catalyst for CO oxidation in a H_2-rich stream†

Yu-Xin Miao, Wen-Cui Li, Qiang Sun, Lei Shi, Lei He, Jing Wang, Gao-Ming Deng and An-Hui Lu*

Manganese oxide-doped Al_2O_3 microspheres were synthesized *via* a redox method, and were then deposited with Au nanoparticles using a deposition–precipitation method. The obtained catalyst is not only highly active and selective for the preferential oxidation of CO in a H_2-rich stream, but also shows excellent stability in the co-presence of H_2O and CO_2 at 80 °C.

Proton exchange membrane fuel cells (PEMFCs) are widely acknowledged as promising candidates to directly convert chemical energy into electricity due to their high energy density and low operating temperature.[1] In fact, the Pt-based electrode of PEMFCs is prone to be poisoned by trace levels of CO in a H_2-rich stream at low temperatures, even at the operating temperatures of 80–120 °C.[2] Hence, the preferential oxidation of CO (CO-PROX) in a H_2-rich stream is accepted as one of the most efficient approaches, which can eliminate trace amounts of CO that poisons the Pt electrode.[3]

Gold catalysts have been demonstrated to show excellent catalytic performance in CO oxidation.[4] However, there are few supported Au catalysts that are able to give a 100% CO conversion, particularly in the temperature range of 80–120 °C, due to the competitive oxidation of H_2.[5] In addition, the catalytic activity and selectivity decrease significantly in the presence of CO_2 and H_2O.[6] Thus, the development of a catalyst system to further enhance the catalytic performance of Au catalysts remains a challenge.

Manganese oxide (MnO_2) is well known as a kind of high oxygen storage capacity material and reducible oxide.[7] It has been shown that MnO_x-based materials can enhance the catalytic activity of a reaction, due to their unique reducibility, and their ability of improving the dispersion of Au nanoparticles.[8] Manganese-modified Au/TiO_2 and Au/CeO_2 catalysts were found to be active for the CO-PROX reaction, while the selectivity at 80–120 °C is rather low (<50%).[9] Recently, we have demonstrated a series of Au/Al_2O_3 catalysts using home-made γ-Al_2O_3 with controlled morphology as efficient supports, which were highly active for CO oxidation,[10] even when CO_2 or/and H_2O were present at room temperature.[11] Therefore, utilizing the advantages of both manganese and alumina to enhance the catalytic activity and stability appears to be very attractive.

Based on the abovementioned state-of-the-art consideration, in this communication, we have developed a very active Au/MnO_2–Al_2O_3 catalyst of which the Al_2O_3 support was synthesized to have organized microsphere structures. Their catalytic performances for CO-PROX were evaluated, which are better than other results reported at 80 °C. Herein, the MnO_2–Al_2O_3 support was synthesized by a redox method and denoted as MnAl. Au nanoparticles, about 1 wt% Au loading, were deposited on such a support by a deposition–precipitation method.[10] The obtained catalyst was denoted Au/MnAl. For comparison, a series of Au/MnO_2, Au/Al_2O_3 and 3 wt% Au/MnO_2–Al_2O_3 catalysts were also prepared and denoted Au/Mn, Au/Al, and 3Au/MnAl, respectively (for details see ESI†).

The morphology and structural information of the synthesized MnAl support and Au/MnAl catalysts were investigated by SEM, TEM, HAADF-STEM and EDX elemental mapping. As shown in Fig. 1a, the Al_2O_3 support shows hollow microsphere structures (the diameter is about 5 to 6 μm) assembled from closely packed nanoflakes. After obtaining doped Mn, the spherical structure of the MnAl supports is retained (Fig. 1b). As seen in the STEM images in Fig. 1c and e, the relative higher contrast of the nanogold in the Z-contrast image indicates that the gold nanoparticles with a narrow size distribution ranging from 2.5 to 7.5 nm are highly dispersed without aggregation. The HRTEM image (Fig. 1d) clearly shows the lattice fringes and well crystallized hexagonal single nanogold. The interplanar distance of the lattice fringes is 0.23 nm corresponding to the Au(111) facets. Furthermore, elemental mapping analysis (Fig. 1f and Fig. S2, ESI†) of the corresponding STEM-EDX data confirms the homogeneous distribution of both Mn and Au atoms in the 3Au/MnAl catalyst.

The XRD patterns reveal (Fig. S1a, ESI†) that all the diffraction peaks of Au/Al and Au/Mn samples are characteristic of the

State Key Laboratory of Fine Chemicals, School of Chemical Engineering, Dalian University of Technology, Dalian 116024, P. R. China.
E-mail: anhuilu@dlut.edu.cn; Fax: +86-411-84986112; Tel: +86-411-84986112

† Electronic supplementary information (ESI) available: Details of catalyst preparation, tests, and some other characterization. See DOI: 10.1039/c5cc06480e

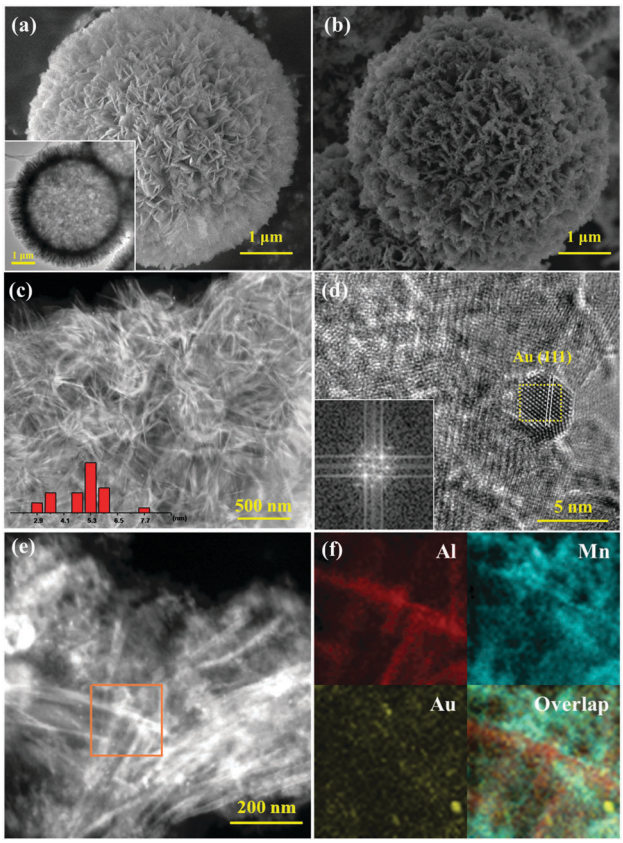

Fig. 1 SEM images of Al_2O_3 (a) and MnAl (b) supports, the inset is the TEM image of Al_2O_3; STEM (c and e) and HRTEM (d) images of the 3Au/MnAl catalyst, the inset is the selected area FFT image; typical EDX maps (f) based on the selected area shown in (e).

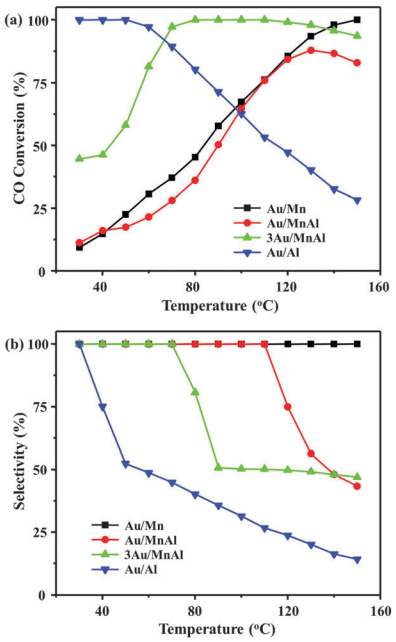

Fig. 2 (a) Conversion and (b) selectivity as a function of the reaction temperature for CO-PROX over different catalysts. Reaction conditions: 1 vol% CO + 1 vol% O_2 + 40 vol% H_2 and balance N_2. Weight hourly space velocity (WHSV) = 40 000 mL h^{-1} g_{cat}^{-1}.

typical γ crystalline phase of alumina (JCPDS, No. 10-0425) and the pure tetragonal phase of MnO_2 (JCPDS, No. 53-0633). In addition, the diffraction peaks of the MnAl supports become broader and less intense, suggesting the existence of mixed phases. It is calculated by using the Bragg's equation that the lattice parameter of MnO_2 in Au/MnAl (0.236 nm) is smaller than that of pure MnO_2 (0.243 nm), indicating that the presence of Mn resulted in the incorporation of Au^+ or Al^{3+} to form a solid solution. Moreover, the characteristic diffraction peaks of Au were not detected, suggesting that the gold nanoparticles were highly dispersed. As observed in Fig. S1b (ESI†), all the catalysts show an IV-type isotherm with type H3 hysteresis loops indicating the presence of mesopores. Table S1 (ESI†) also indicated that the BET surface area and pore structure of Au/Al and Au/MnAl catalysts were only slightly affected by doping with manganese. The compositions of these catalysts were quantitatively analyzed by ICP-AES, and the results indicated that the metallic contents are very close to the theoretical values. Thus, based on the above results, one can conclude that the highly dispersed Au nanoparticles on the MnAl support have been synthesized.

Fig. 2a and b shows the catalytic activity and selectivity for CO-PROX of the different Au catalysts. It can be clearly seen that the Au/Al catalyst shows the maximum CO conversion of 100% at 30–50 °C and has the highest activity, but it dramatically decreased due to the occurrence of H_2 oxidation when the CO-PROX reaction temperature was increased. However, the Au/Mn catalyst was almost inactive at 30 °C but the CO conversion gradually increased with temperature and reached 100% at a higher temperature of 150 °C. Compared to the Au/Al catalyst, Au/Mn and Au/MnAl catalysts are found to be less active for CO-PROX, however more selective at the operation temperature after doping with manganese. Upon increasing the theoretical loading of the Au content from 1% to 3%, the 3Au/MnAl catalyst exhibited a wide temperature window of 100% CO conversion at 80–120 °C, and the selectivity of CO_2 was nearly 80% at 80 °C. It should be noted that in the operating temperature range of 80–120 °C 3Au/MnAl is more active than 3Au/Al and 3Au/Mn (Fig. S3, ESI†). These improved catalytic performances provide clear evidence of a strong interaction between gold and manganese. Furthermore, in comparison with those Au catalysts published recently (Table S2, ESI†), our catalyst is the most active one for CO-PROX.[12]

The stability test of the 3Au/MnAl catalyst was conducted in the absence or presence of H_2O and CO_2. From Fig. S4a (ESI†), it is observed that the catalyst can be very stable without the addition of H_2O and CO_2. After adding 10 vol% H_2O and 20 vol% CO_2, the conversion of CO still remained 95% after consecutive runs for 40 h at 80 °C and the catalytic selectivity was decreased from 80% to 55% and then reached the steady state. In order to understand the effect of H_2O and CO_2, the catalytic activities of sample 3Au/MnAl with temperature in the presence of H_2O and/or CO_2 were separately investigated (Fig. S4b and c, ESI†). A negative effect on the activity for CO-PROX caused by CO_2 was observed. The XRD pattern of the spent 3Au/MnAl catalyst is presented in Fig. S1a (ESI†). Comparing to the fresh catalyst, the intensities of MnO_2 diffractions

at 38.1° (211) and 44.3° (321) slightly decreased and the mean Mn crystallite size increased from 26 nm (fresh 3Au/MnAl) to 34 nm (used 3Au/MnAl) as calculated by the Scherrer's equation. In addition, diffraction peaks assigned to manganese carbonate (JCPDS, No. 44-1472) were observed. This may suggest that the carbonate species formed on the spent catalyst surface caused the catalyst deactivation.

To understand the exceptionally high catalytic activity and selectivity of the Au catalysts, DRIFTS characterization of CO adsorption was chosen to study the surface adsorption behavior. As shown in Fig. S5 (ESI†), similar vibration bands at 2056, 2114, and 2171 cm^{-1} were observed for Au/Al, Au/Mn and Au/MnAl catalysts, which can be accordingly ascribed to the CO adsorption on $Au^{\delta-}$, Au^0 and $Au^{\delta+}$.[11,13] The intensity of peaks at 2056 cm^{-1} on various Au catalysts follows the order of Au/Al > 3Au/MnAl > Au/MnAl > Au/Mn. The results indicate that the increase of the Au content on MnAl support can enhance CO adsorption, thus promoting the catalytic performance for CO-PROX at higher reaction temperatures.

The H_2-TPR was tested to further understand the relative reducibility corresponding to its catalytic performance (Fig. 3a). For the Au/Al sample, only one weak reduction peak at 227 °C can be ascribed to the reduction of the Au_xO_y species to metal Au (Au^0). For the Au/Mn catalyst, two reduction peaks were found at low temperatures, *i.e.* 267 and 321 °C, which can be attributed to the reduction of MnO_2 to Mn_3O_4 and Mn_3O_4 to MnO, respectively.[7a,14] In the case of the Au/MnAl catalyst, the two reduction peaks shifted toward higher temperatures (275 and 377 °C). This might correspond to the less dispersed Mn in the mixed oxides or weaker interaction on the support surface. Similar results were also reported for the Ni/CeO_2–ZrO_2 and Au/CeO_2–Fe_2O_3 catalysts.[15] Furthermore, the presence of Au nanoparticles can improve the reducibility of the 3Au/MnAl catalyst by shifting the reduction peaks toward lower temperature (200 and 339 °C) as compared to the MnAl support and Au/Mn catalysts. It indicates the presence of strong interaction between Au and MnAl support.

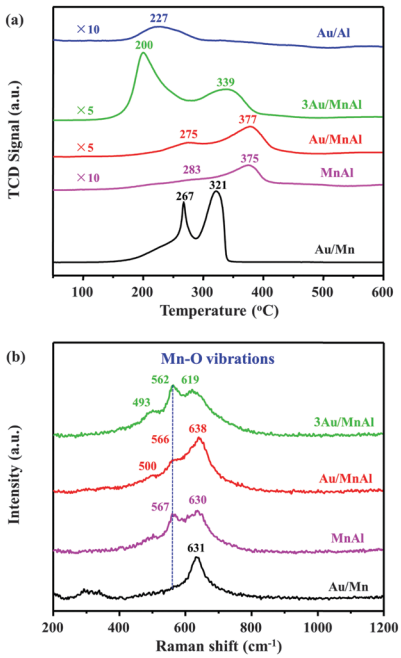

Fig. 3 (a) H_2-TPR profiles and (b) Raman scattering spectra of Au catalysts.

To further obtain more information on the structure of the Au/MnAl catalyst, Raman spectra excited by a 532 nm laser were recorded. The Raman spectra (Fig. 3b) show that the bands at around 500, 566 and 638 cm^{-1} were attributed to the characteristic spectral features of the typical α-MnO_2 phase.[16] The strong bands at *ca.* 580–632 cm^{-1} have been associated with the symmetrical Mn–O vibrations and indicated the well-developed tetragonal and octahedral structure.[17] For the 3Au/MnAl catalyst, the $6A_g$ band (*ca.* 562 cm^{-1}) is always broader than that of the Au/MnAl and MnAl samples. In addition, the band shifts towards lower frequencies (from 638 to 619 cm^{-1}), especially in the case of the Au/MnAl catalysts with a higher Au content. Meanwhile, the intensity of the strong bands at 566 cm^{-1} assigned to the symmetrical Mn–O vibrations was increased. This suggests that strong Au–O–Mn bonds may be generated on the interface of MnAl support. In our case, we can infer that the strong interaction of gold with manganese could be the reason for the strong Raman shift and higher width of the $6A_g$ band in the 3Au/MnAl sample compared with those in Au/MnAl. Furthermore, the XPS results (Fig. S6, ESI†) prove that there exists electron transfer between Au^0 and Mn^{4+} for the 3Au/MnAl catalyst with the formation of $Au^{\delta+}$ and Mn^{3+}. This indicated a strong interaction between the gold and the support. The result is in good agreement with the H_2-TPR studies discussed above. Combining the catalytic activity results (Fig. 2a), we speculate that the highly catalytic activity for CO-PROX reaction is due to the enhanced Au–O–Mn interaction and high reducibility of the 3Au/MnAl catalyst. For clarity, the "structure–activity" relationship model of the Au/MnAl catalysts is shown in Scheme S1 (ESI†). Similarly, the high activity for the CO-PROX has also been observed in the 3Au/MnCe and 3Au/MnAl (without hollow structure) catalysts, indicating the positive effect of Mn modification on the gold catalysts (Fig. S7, ESI†).

In summary, we have synthesized an Au/MnO_2–Al_2O_3 catalyst with organized microsphere structures. By means of various catalytic characterization techniques, fine nanogold was highly dispersed on the MnAl support. Benefiting from the strong Au–support interaction and reducibility, the resulting 3Au/MnAl exhibits rather high activity (100% CO conversion) and selectivity (80%, 80 °C) for CO-PROX, compared to the reported catalysts. In addition, it also shows one wide temperature range (80–120 °C) for full CO conversion under the PEMFC operation conditions and displays excellent catalytic stability even under the co-presence of H_2O and CO_2 at 80 °C (95% CO conversion). We believe that the proposed manganese oxide-doped Al_2O_3 supported nanogold here may open up new opportunities for the development of active gold catalysts for CO-PROX and other reactions.

The authors would like to acknowledge the financial support from the National Program on Key Basic Research Project (No. 2013CB934104) and the National Natural Science Foundation of China (No. U1462120 and 21225312).

Notes and references

1 (*a*) A. Biyikoglu, *Int. J. Hydrogen Energy*, 2005, **30**, 1181; (*b*) A. F. Ghenciu, *Curr. Opin. Solid State Mater. Sci.*, 2002, **6**, 389.

2 (*a*) T. V. Choudhary and D. W. Goodman, *Catal. Today*, 2002, **77**, 65; (*b*) B. C. H. Steele and A. Heinzel, *Nature*, 2001, **414**, 345.

3 (*a*) S. Huang, K. Hara and A. Fukuoka, *Energy Environ. Sci.*, 2009, **2**, 1060; (*b*) K. Liu, A. Wang and T. Zhang, *ACS Catal.*, 2012, **2**, 1165.

4 (*a*) A. S. K. Hashmi and G. J. Hutchings, *Angew. Chem., Int. Ed.*, 2006, **45**, 7896; (*b*) M. Daté, M. Okumura, S. Tsubota and M. Haruta, *Angew. Chem., Int. Ed.*, 2004, **43**, 2129.

5 (*a*) P. Landon, J. Ferguson, B. E. Solsona, T. Garcia, A. F. Carley, A. A. Herzing, C. J. Kiely, S. E. Golunski and G. J. Hutchings, *Chem. Commun.*, 2005, 3385; (*b*) Q. Lin, B. Qiao, Y. Huang, L. Li, J. Lin, X. Y. Liu, A. Wang, W.-C. Li and T. Zhang, *Chem. Commun.*, 2014, **50**, 2721; (*c*) J. A. Hernández, S. A. Gomez, T. A. Zepeda, J. C. Fierro-González and G. A. Fuentes, *ACS Catal.*, 2015, **5**, 4003; (*d*) Y. Liu, B. Liu, Q. Wang, C. Li, W. Hu, Y. Liu, P. Jing, W. Zhao and J. Zhang, *J. Catal.*, 2012, **296**, 65.

6 (*a*) E. O. Jardim, S. Rico-Francés, F. Coloma, E. V. Ramos-Fernández, J. Silvestre-Albero and A. Sepúlveda-Escribano, *Appl. Catal., A*, 2014, **487**, 119; (*b*) A. Luengnaruemitchai, S. Chawla and R. Wanchanthuek, *Int. J. Hydrogen Energy*, 2014, **39**, 16953; (*c*) N. Bion, F. Epron, M. Moreno, F. Mariño and D. Duprez, *Top. Catal.*, 2008, **51**, 76.

7 (*a*) M. Alhumaimess, Z. Lin, Q. He, L. Lu, N. Dimitratos, N. F. Dummer, M. Conte, S. H. Taylor, J. K. Bartley, C. J. Kiely and G. J. Hutchings, *Chem. – Eur. J.*, 2014, **20**, 1701; (*b*) Z.-Y. Fei, B. Sun, L. Zhao, W.-J. Ji and C.-T. Au, *Chem. – Eur. J.*, 2013, **19**, 6480.

8 (*a*) Y.-X. Miao, L.-H. Ren, L. Shi and W.-C. Li, *RSC Adv.*, 2015, **5**, 62732; (*b*) A. Luengnaruemitchai, D. T. K. Thoa, S. Osuwan and E. Gulari, *Int. J. Hydrogen Energy*, 2005, **30**, 981.

9 (*a*) L.-H. Chang, N. Sasirekha and Y.-W. Chen, *Catal. Commun.*, 2007, **8**, 1702; (*b*) L.-H. Chang, N. Sasirekha, Y.-W. Chen and W.-J. Wang, *Ind. Eng. Chem. Res.*, 2006, **45**, 4927; (*c*) M. Meng, Y. Tu, T. Ding, Z. Sun and L. Zhang, *Int. J. Hydrogen Energy*, 2011, **36**, 9139.

10 (*a*) J. Wang, K. Shang, Y. Guo and W.-C. Li, *Microporous Mesoporous Mater.*, 2013, **181**, 141; (*b*) J. Wang, A.-H. Lu, M. Li, W. Zhang, Y.-S. Chen, D.-X. Tian and W.-C. Li, *ACS Nano*, 2013, **7**, 4902.

11 Y.-X. Miao, L. Shi, L.-N. Cai and W.-C. Li, *Gold Bull.*, 2014, **47**, 275.

12 P. Lakshmanan, J. E. Park and E. D. Park, *Catal. Surv. Asia*, 2014, **18**, 75.

13 (*a*) X. Liu, M.-H. Liu, Y.-C. Luo, C.-Y. Mou, S. D. Lin, H. Cheng, J.-M. Chen, J.-F. Lee and T.-S. Lin, *J. Am. Chem. Soc.*, 2012, **134**, 10251; (*b*) T. Venkov, H. Klimev, M. A. Centeno, J. A. Odriozola and K. Hadjiivanov, *Catal. Commun.*, 2006, **7**, 308.

14 (*a*) R. Xu, X. Wang, D. Wang, K. Zhou and Y. Li, *J. Catal.*, 2006, **237**, 426; (*b*) J. Li, L. Li, F. Wu, L. Zhang and X. Liu, *Catal. Commun.*, 2013, **31**, 52.

15 (*a*) P. Biswas and D. Kunzru, *Int. J. Hydrogen Energy*, 2007, **32**, 969; (*b*) C. Pojanavaraphan, A. Luengnaruemitchai and E. Gulari, *Int. J. Hydrogen Energy*, 2012, **37**, 14072.

16 (*a*) S. Cheng, L. Yang, D. Chen, X. Ji, Z.-J. Jiang, D. Ding and M. Liu, *Nano Energy*, 2014, **9**, 161; (*b*) J. Luo, H. T. Zhu, H. M. Fan, J. K. Liang, H. L. Shi, G. H. Rao, J. B. Li, Z. M. Du and Z. X. Shen, *J. Phys. Chem. C*, 2008, **112**, 12594; (*c*) T. Gao, H. Fjellvåg and P. Norby, *Anal. Chim. Acta*, 2009, **648**, 235.

17 (*a*) K. Selvakumar, S. M. S. Kumar, R. Thangamuthu, K. Ganesan, P. Murugan, P. Rajput, S. N. Jha and D. Bhattacharyya, *J. Phys. Chem. C*, 2015, **119**, 6604; (*b*) T. Gao, M. Glerup, F. Krumeich, R. Nesper, H. Fjellvåg and P. Norby, *J. Phys. Chem. C*, 2008, **112**, 13134.